ANALYSIS AND IMPROVEMENT OF SINGLE-PHASE FLOW FIELD INSIDE THE CRUSHING CHAMBER OF MACHINE FOR LENTINUS EDODES STIPE CRUSHING
/
香菇柄成松机成松室内单相流场分析与改进

Yang LI [1,2], Yanjun LI [3], Pei LI [4] [1]

[1] Chinese Academy of Agricultural Mechanization Sciences Group Company Limited, Beijing 100083, China
[2] National Key Laboratory of Agricultural Equipment Technology, Beijing 100083, China
[3] Weifang University, Weifang, Shandong 261061, China
[4] Shandong University of Technology, Zibo, Shandong 255000, China
Tel: +86-18811778308; E-mail: tanfeiyuxie@163.com
DOI: https://doi.org/10.35633/inmateh-69-67A

Keywords: *FLUENT; simulation; machine for lentinus edodes stipe crushing; flow field.*

ABSTRACT

In order to analyze the flow field inside the crushing chamber of machine for lentinus edodes stipe crushing and improve performance of the machine based on the results of the flow field analysis, this paper applied the computational fluid dynamics software FLUENT to numerically simulate the flow field inside the crushing chamber of the machine for lentinus edodes stipe crushing. Thus, the flow field characteristics and flow state inside the crushing chamber were intuitively displayed, and the visualization of the flow field in the crushing chamber was realized. Then, the wind speed value obtained by simulation was compared with the value measured by experiment, and the average relative error between them was less than 10%. Finally, according to the simulation results of flow field, the flow field generated by one air inlet and two air inlets was analyzed, and then the blade structure, outlet area parameters, and rotation speed parameters were compared, simulated and optimized. Results analysis: the pressure distribution and velocity distribution of the flow field inside the crushing chamber were obtained, and the optimal structure and parameters were two inlets, the rotation speed of 2000 r/min and the outlet area of 160×80 mm^2, the crushing chamber with the new blade parameters and structure had greater turbulent kinetic energy and velocity gradient, which was more favorable to the discharge, and provided a basis for further optimization and improvement of the crushing machine.

摘 要

为了对香菇柄成松室进行内部流场分析以及根据流场分析结果对成松室进行改进，本文应用计算流体力学软件 FLUENT 对香菇柄成松机成松室的内部流场进行数值模拟，从而直观显示了成松机腔体内的流场特性和流动状态，实现了成松室流场的可视化。然后对仿真所得的风速值和试验测得的值进行对比，得出二者平均相对误差小于 10%，最后根据流场模拟结果，对一个进风口和两个进风口内流场进行分析，然后对刀片结构，出料口面积参数，转速参数进行对比模拟分析优化。结果分析:得到了成松室内流场的压力分布和内部流场速度分布，并依据仿真结果得到两个进风口，转速为 2000r/min，出料口面积为 160×80 ㎜^{2}，新型刀片的参数与结构下的成松室具有更大的湍动能和速度梯度，更有利于出料，并为成松机的进一步优化改进提供基础。

INTRODUCTION

Lentinus edodes stipe is hard to chew, but it has high nutritional value, so the group has developed the machine for lentinus edodes stipe crushing, whose key component, the striking device, is cleverly designed and consists of 72 blades, 18 discs and 17 sleeves through the spiral mounting structure, which can well realize the striking and conveying of materials. The working principle of the machine for lentinus edodes stipe crushing is that the lentinus edodes stipe is broken up and formed into a crushed shape conforming to the quality evaluation standard through the collision and rubbing effect between the high-speed rotating blades and the materials by using the striking principle, and is discharged from the outlet through the centrifugal fan (*Liu Liangdong, 2016*). So, the machine for lentinus edodes stipe crushing can realize the industrialization and large-scale production, and the effect of lentinus edodes stipe crushing is also good, which has greater economic and social benefits, so the in-depth research on the machine for lentinus edodes stipe crushing also becomes important.

[1] *Yang LI*, Ph.D. Stud. Eng.; Yanjun LI, Ph.D. Stud. Eng.; Pei LI, Ph.D. Stud. Eng.*

As the material inside the crushing chamber is highly susceptible to the influence of the internal airflow, the magnitude of the internal airflow also affects the material discharge and the lentinus edodes stipe crushing effect of the crushing chamber.

In addition to this, the crushing efficiency is largely constrained by the internal circulation layer (*Wang Xiaofeng, 2008*), resulting in low crushing efficiency and high energy consumption of the crushing machine. However, the complex flow field inside the crushing chamber cannot be viewed with the naked eye, so numerical simulation is an effective method to study the complex flow field inside the equipment in depth (*Darelius A. et al, 2008; Barailler F. et al, 2006*). Canadian scholar Dennis Ramo simulated the airflow field distribution inside a traction forage harvester on FLUENT 6.1 (*Lammers, 2005*). Gong Jun from Lanzhou University of Technology performed FLUENT numerical simulation of the flow field inside the pulverizing chamber of a turbulent ultrafine pulverizer with different leaf types, and the simulation results clearly demonstrated the flow field structure inside the pulverizing chamber (*Gong Jun, et al, 2006*). *Peiyu Shen et al* used FLUENT software to simulate the flow field inside the high-speed cutting and crushing chamber of agricultural materials and derived the pressure and velocity distribution of the internal flow field as well as the optimal impeller blade shape and blade deflection angle and impeller speed (*Shen Peiyu et al, 2010)*. Due to the complex internal flow field of the machine for lentinus edodes stipe crushing, it is difficult to obtain it by experimental means or other methods. In this paper, the internal flow field distribution is numerically simulated by using Fluent, a fluid dynamics software, and the distribution state of the internal flow field is obtained by analyzing the flow field in it, and some structural parameters and operation parameters are improved to provide the basis for further optimization of the machine for lentinus edodes stipe crushing.

MATERIALS AND METHODS

The overall design of prototype

- **Prototype introduction**

The machine for lentinus edodes stipe crushing developed by the group was used as the research object, in which the structure of the machine is shown in Figure 1. The crushing machine adopts the principle of forming lentinus edodes stipe floss by striking, after the lentinus edodes stipe is treated by the pre-treatment process, the lentinus edodes stipe is added into the cylinder inside the housing through the feed hopper, and the lentinus edodes stipe is moved to the outlet under the negative pressure generated by the fan and the striking and pushing action of the rotor device, during the moving process, the high-speed rotating blades collide and knead with the lentinus edodes stipe repeatedly, so as to break the lentinus edodes stipe into a fine stipe shape and realize the soft formation of the lentinus edodes stipe. The lentinus edodes stipe is crushed and the crushed lentinus edodes stipe is discharged through the discharge port for post-processing to obtain the required lentinus edodes stipe floss. The generated dust is discharged from the machine through the centrifugal dust collector.

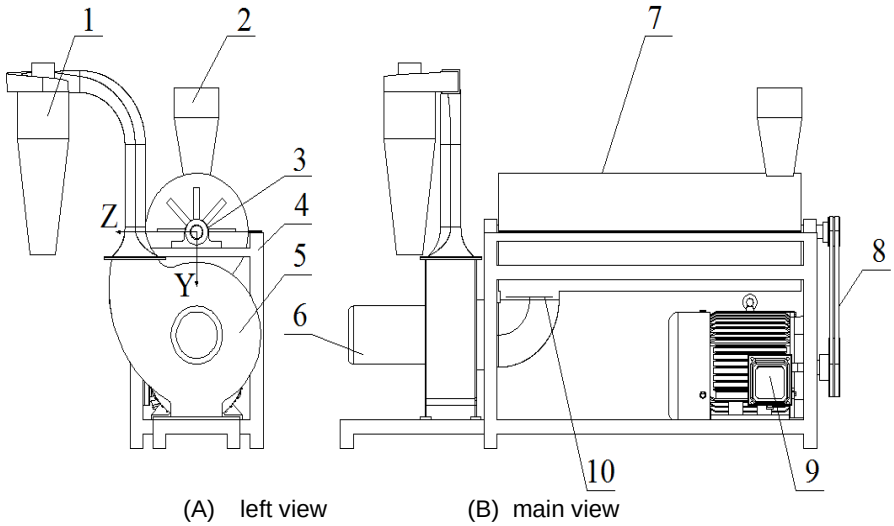

Fig. 1 - Structure of the machine for lentinus edodes stipe crushing
1. Centrifugal dust collector; 2. Feed hopper; 3. Rotor; 4. Frame; 5. Fan; 6. fan motor; 7. Shell; 8. Belt drive; 9. Main motor; 10. Discharge port

Table 1

Parameters of the crushing chamber of the machine for lentinus edodes stipe crushing

Mating power (kW)	3
Rotation Speed (r/min)	2200
Number of blades	72
The distance between the end of the blade and the cylinder (mm)	7
Discharge port area (mm^2)	160×80
Sleeve length (mm)	50
Blade thickness (mm)	5
Tool Type	Straight Blade

Theoretical calculation method

- **Mathematical model**

The comparison between the Reynolds number and the boundary Reynolds number is used to determine whether the flow inside the crushing chamber is turbulent or laminar. The measured velocity at the outlet is 21.14 m/s, and the Reynolds number is calculated from Equation (1) (*Huang Yihui, 2011*).

$$\mathrm{Re} = \frac{vd}{V} \tag{1}$$

where: v - velocity; d - inlet hydrodynamic diameter; V - aerodynamic viscosity.

$$d = \frac{2ab}{a+b} \tag{2}$$

where: a, b are the length and width of the rectangle of the exit section.

From the formula (2), it can be derived from the exit of the hydraulic diameter of 106.67mm, and the standard aerodynamic viscosity is 15×10^{-6} m^2/s, so the airflow Reynolds number at the exit is 1.5×10^5, the Reynolds number is greater than 2300, that is, it belongs to turbulent flow.

Secondly, we define the coordinates of the crushing chamber to clarify the X, Y and Z directions of the machine, so as to facilitate the analysis and verification of the velocity-pressure clouds and the velocity of the points on the opposite side.

X - the direction in which the spindle is located.

Y-direction perpendicular to the inlet and outlet, i.e. radial direction.

Z-direction perpendicular to X-axis, Y-axis.

The study is solved numerically using the standard k-e model with the control equations including the mass conservation equation, the momentum conservation equation, the turbulent kinetic energy k equation and the dissipation rate equation, which are expressed as the following general equations (*Wang Juan et al, 2010; Zhai Zhiping et al, 2008*):

$$\frac{\partial(\rho\phi)}{\partial t} + \frac{\partial(\rho u\phi)}{\partial x} + \frac{\partial(\rho v\phi)}{\partial y} + \frac{\partial(\rho w\phi)}{\partial z} = \frac{\partial}{\partial x}\left(\Gamma\frac{\partial\phi}{\partial x}\right) + \frac{\partial}{\partial y}\left(\Gamma\frac{\partial\phi}{\partial y}\right) + \frac{\partial}{\partial z}\left(\Gamma\frac{\partial\phi}{\partial z}\right) + S \tag{3}$$

where:

$\emptyset$ - generalized variable; Γ - diffusion coefficient; S - source term;

u-x velocity in x direction; v-y velocity in Y direction; w-z velocity in Z direction; ρ - density; t - time.

- **Calculation area and mesh generation**

The complexity of the flow channel model is simplified by considering the crushing chamber as a completely closed area and omitting all the small gaps and chamfers (*Cao Liying et al, 2010*). The shaft and blade set as a whole, omitting the connections between each structure, the small gaps between the blades and the cutterhead, between the blades and the shaft and between the sleeve and the shaft do not affect the magnitude of the negative pressure in the flow field, so the shaft and blades set can be built directly as a single body.

Boolean subtraction operations were performed on the whole model to cut out the flow paths to form the rotational and stationary domains (*Zhu Lianhua et al, 2015)*. The fluid medium in the simulation is air with a density of 1.225 kg/m^3, and the air flow space of the crushing chamber is selected as the calculation region, i.e., the air flow enters from the inlet and exits from the outlet of the crushing chamber.

The model created with the 3D software PROE, as shown in Figure 2, is imported into the pre-processing software ICEM CFD of FLUENT for meshing. The whole calculation area is divided into five parts, namely two inlet runners, outlet runners, rotor set runners, and circular housing runners. Due to the spatial complexity of the computational region, the mesh division uses a more adaptable non-structural tetrahedral mesh (*Cao Yuan et al, 2015)*. After the grid division is completed, the quality of the grid is also checked, and the quality of the grid is still checked mainly by the numerical cells of Equisize Skew and Minimum Value, which is the minimum volume of the cell and requires that it must be greater than 1, otherwise it cannot be used (*Qianpu Wang et al, 2001; Robert Johansson et al, 2014; Bo Yuan Lim et al, 2016*). According to the size of the area using different sizes of the grid, the whole crushing chamber is divided into a total of 1965284 cells, the model after the grid division is shown in Figure 3.

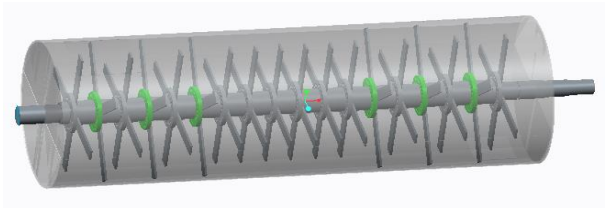

Fig. 2 - Three dimensional geometric solid model of the crushing chamber

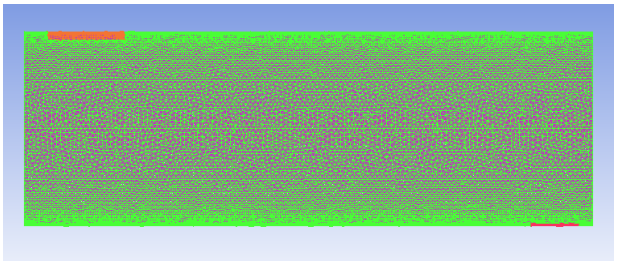

Fig. 3 - Meshing of computational region

- **Multiple coordinate reference systems and boundary conditions**

The FLUENT software provides three models describing the rotational motion of fluids: the multi-reference system model, the slip mesh model, and the dynamic mesh model to deal with the case of relative motion between multiple objects, which are widely used for solving problems of turbine engines, impeller machinery, and mixing apparatus (*Song Yongqi, 2007*).The MRF model is a calculation method based on the steady-state flow field (*Li Weidong et al, 2017*) and is the simplest of the rotation models, which divides the computational domain into a rotating part and a stationary part, and uses the rotating and stationary coordinate systems to perform the calculation separately, without the need for internal and external iterations, thus saving computational time. The MRF model reduces the flow field inside the crushing chamber to a transient flow field of the blades at a given location (*Shang Tan et al, 2014*) .While the sliding grid model and the dynamic grid model are suitable for calculating the unsteady flow field, the calculation time is long (*Pei Yaowu, 2014*), for the simulation and analysis of the relatively simple rotating model, this rotating flow field can be simulated approximately with the MRF model, and the same results can be obtained to match the actual situation. In this paper, multiple reference coordinate systems are used for the calculation, which requires the establishment of interface surfaces between the moving and stationary regions for energy transfer. The rotor group area is established on the kinematic reference system, and the rest of the wall area such as the shell area is established on the fixed coordinate system.

The inlet and outlet of the crushing chamber are the pressure inlet and pressure outlet respectively. The default setting is used for the pressure inlet, and the pressure measured at the pressure outlet is 940Pa.

- **Numerical calculation method**

The calculations are performed using the standard k-e model with no-slip wall boundary conditions, i.e., the relative velocity is zero (*Zong Quanli et al, 2013*). The flow simulation in the near-wall region was performed using standard wall functions and the pressure-velocity coupling was solved using the standard SIMPLE algorithm (*R. Aghaei tog et al, 2008; Guo Yuhang, 2015*).

The convergence was dynamically monitored by checking the residuals during the solution process, with a convergence accuracy of 0.001. The setting of the relaxation factor should also be reasonable, too high for the analysis to converge and too low to maintain accuracy.

RESULTS AND ANALYSIS

Simulation test

The numerical calculation converges at 765 steps and the calculation is completed. For the analysis, the point (0.648, 0.03, -0.03) is used as the coordinates of the center point of the crushing cylinder, and the central section of the Z-axis including the inlet and outlet is selected to analyze the flow field with the flow of air in the inlet and outlet. In addition, to analyze the pressure and velocity distribution in the vicinity of the blade, a cross-section including the blade was selected for analysis, so one of the cross sections with X=0.674 was chosen, which shows the distribution of the flow field into the cylinder after the Boolean operation on the blade and has obvious characteristics of easy analysis. From Fig.4, it can be seen that the entire crushing cylinder is in a negative pressure state, and the absolute value of wind pressure increases from the inlet to the outlet in order. This can ensure that the material in the process of conveying is relatively smooth, but also can make the lentinus edodes stipe floss has met the requirements of the smooth discharge rather than being repeatedly struck into powder.

In addition, it can be seen from Figs.5 and 6 that the airflow velocity at the tip of the blade is maximum, and then gradually decreases until it reaches 0 in the area where it will reach the shell area. This is because the rotation of the blade drives the fluid to rotate together, thus generating centrifugal force, and when the gas flows in the cylinder, the linear velocity of the fluid increases as the radius increases, and the energy gained by the fluid increases.

Fig.7 shows that the negative pressure at the center of the rotor has a pattern, the closer to the center, the greater the negative pressure value. And in the near the cylinder wall due to the high-speed rotation of the blade generated by the centrifugal force, resulting in the near-wall area of the pressure value is relatively small. And from the figure can also be derived from the blade near the tip, the blade back wind side of the negative pressure is larger, while in the blade tip windward side of the negative pressure is smaller, so that the entire blade pressure difference. The back of the knife tip is a suction surface, and the negative pressure inside the entire cylinder is superimposed, resulting in a greater negative pressure on the back. Fig. 8 shows the velocity vector diagram of the whole crushing cylinder, from which the trajectory of the fluid can be seen. With the high-speed rotating motion of the blade, the fluid is in a spiral motion in the crushing cylinder, instead of just rotating, which just reflects the conveying role of this crushing machine and is also in line with the actual situation.

Fig.9 shows the velocity distribution in axial and radial positions at a speed of 2200 r/min obtained by numerical simulation. The graph shows that the velocity of the fluid is smaller at the position close to the spindle, but as the distance from the spindle increases, the velocity of the fluid also starts to increase, except that it starts to increase slowly at about 68 mm from the barrel wall, and then increases more rapidly, while at the tip of the tool, the linear velocity reaches its maximum. In the gap between the end of the blade and the cylinder wall, the velocity of the fluid decreases dramatically because the blade has difficulty in applying the required kinetic energy to the fluid, resulting in a distinct "cliff structure" (*Zhang Hongwei, 2013*). As shown in Figure 9(b), the fluid velocity is small and varies gently in the area between the blades, while it is larger in the area above the blades.

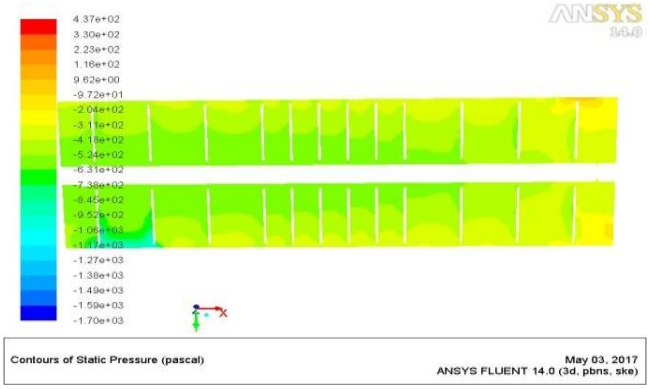

Fig. 4 - Pressure contour plot at plane position Z=-0.03m

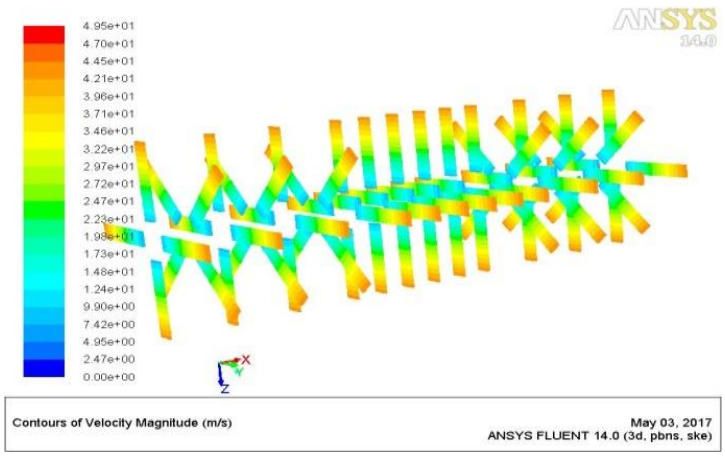

Fig. 5 - Velocity contour for the blade group

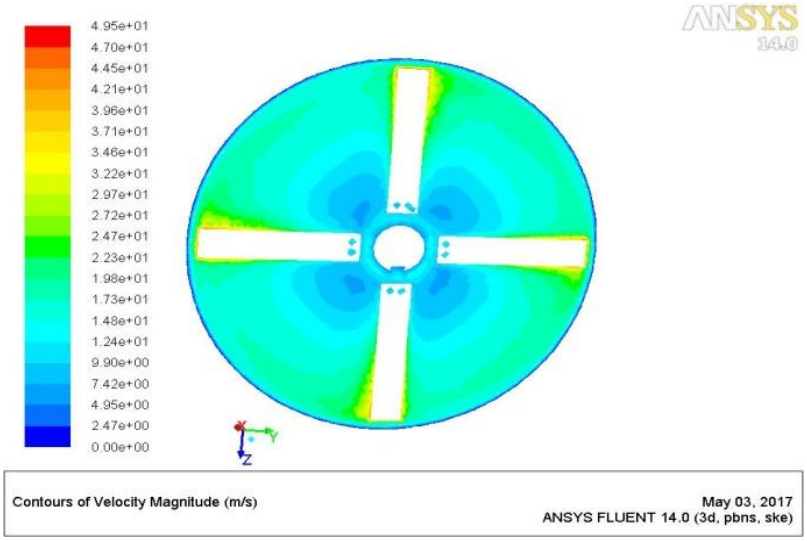

Fig. 6 - Velocity contour plot at plane position X=0.674m

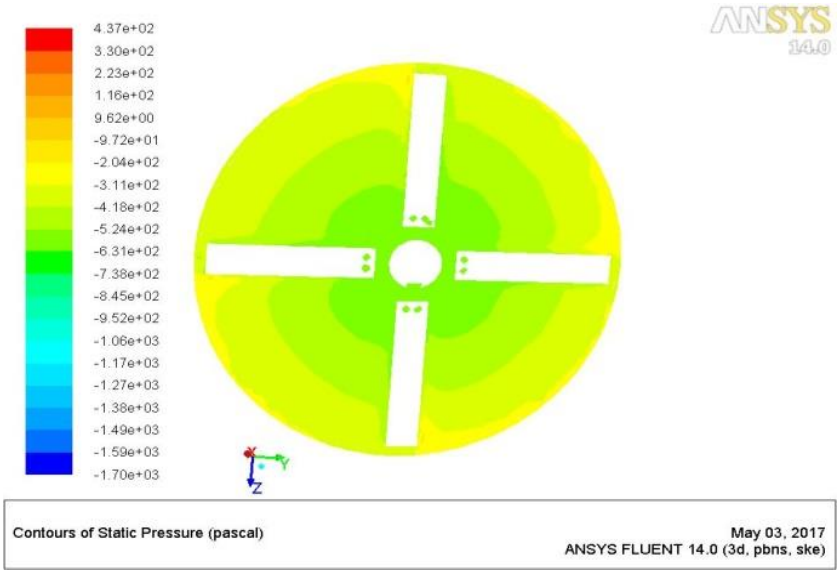

Fig. 7 - Pressure contour plot at plane position X=0.674m

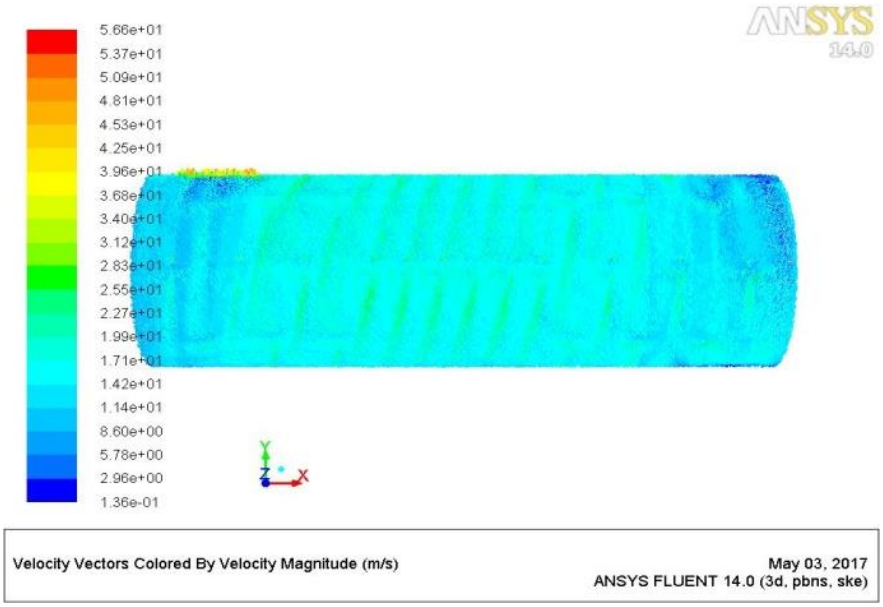

Fig. 8 - Velocity vector for the crushing cylinder

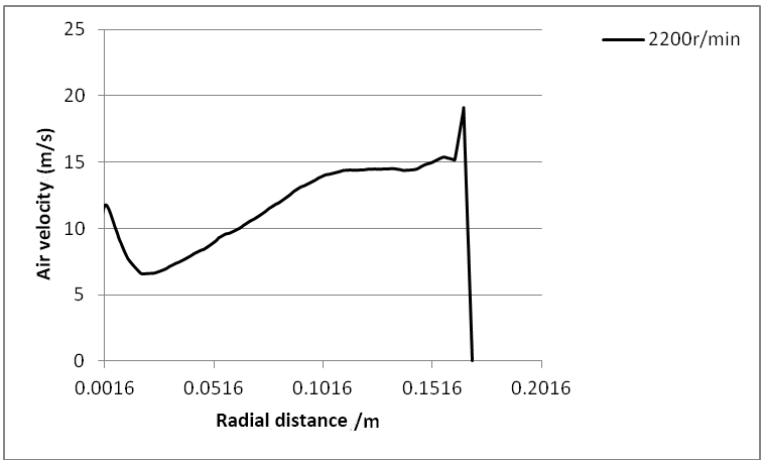

(a) Variation of the velocity inside the crushing chamber from the rotating shaft to the cylinder wall

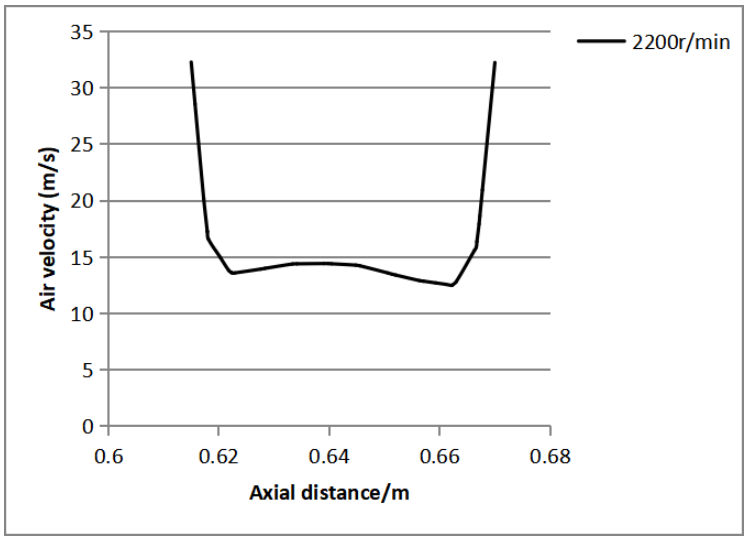

(b) Variation of fluid velocity along the axial direction between adjacent blades

Fig. 9 - Velocity distribution at a 2200r/min shaft speeds for the crushing chamber

Verification of the correctness of the numerical simulation method

- **Experimental validation**

(1) Test instrument and measurement point arrangement

In order to test the reliability of the simulation, the airflow speed at the measurement point was measured under no-load conditions at 1800r/min, 2000r/min and 2200r/min, respectively, using a KXYL-600B digital pressure-velocity-airflow meter under the simultaneous rotation of the fan motor and the spindle motor.

The measurement points are measured as follows: the Pitot cylinder is fixed on the upper part of the cylinder wall, and the position of the Pitot cylinder inside the cylinder is changed by adjusting the clamps in the up and down direction to measure the fluid velocity at different spatial points. The position is mainly measured by vernier calipers, and the value is taken every 5 mm along the Y direction between the two blades in the middle of the cylinder, as shown in Fig.10.

The coordinates of the measured points should correspond to the coordinates of the numerical simulation to compare the error between the test value and the simulation value. The coordinates of each measurement point are:1:(0.648,-0.11,-0.03)2: (0.648,-0.115,-0.03)3: (0.648,-0.12,-0.03)4: (0.648,-0.125,-0.03)5: (0.648,-0.13,-0.03)6:(0.648,-0.135,-0.03)7:(0.648,-0.14,-0.03)8:(0.648,-0.145,-0.03)9:(0.648,-0.15,-0.03)10:(0.648,-0.155,-0.03)11:(0.648,-0.16,-0.03)12:(0.648,-0.165,-0.03).

Each measurement point was repeated at least three times and the average of the three test results was recorded. The experimental equipment for measuring the airflow velocity in the crushing chamber is shown in Fig.11.

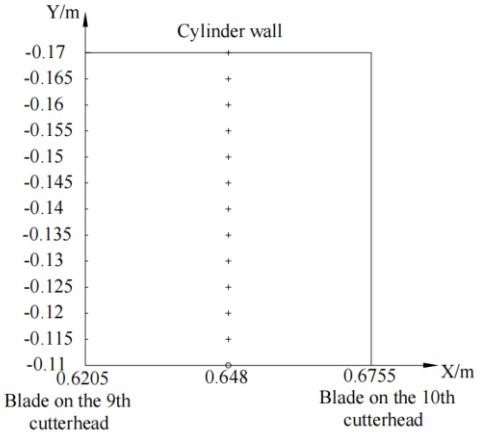

Fig. 10 - The layout of measurement positions for fluent velocities

Fig. 11 - Experimental equipment for measuring fluid velocities of flow field in the crushing chamber

(2) Comparative analysis of test results and simulation results

The test results measured along the radial direction of the crushing chamber were compared with the simulated results, as shown in Fig. 12. From the figure, it can be seen that the trend of the velocity distribution obtained from the simulation is the same as the test value, except that the simulated velocity value is larger, which is because the simulation is carried out under ideal conditions, ignoring factors such as air leakage and friction between the airflow and the blade and wall surface. The exit velocity is measured for

different outlet areas and speeds to further verify the simulation results. To further verify the simulation results, this paper makes further verification for different outlet areas and different speeds, measures the speed at the center of the outlet, and compares the area-weighted average outlet speed obtained from the simulation with the actual measured outlet speed at the center, as shown in Table 2, the average relative error between the simulated speed value and the actual measured speed value is about 10%, which proves that the simulation results are feasible.

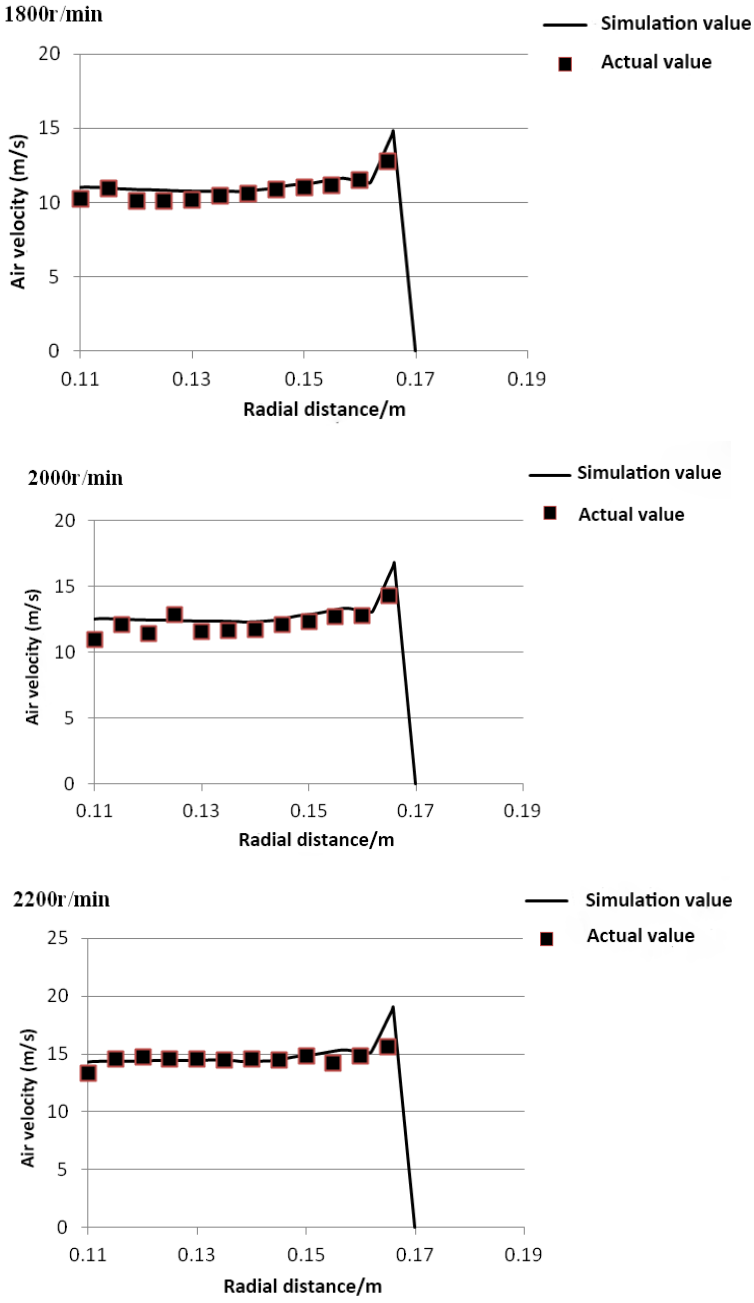

Fig.12. Comparison between measured and simulated results of air velocity measured by Y to each measuring point

Table 2

Comparison of simulation and measured velocity at different speeds and outlets

Rotational Speed(rpm)	Discharge port area(mm²)	Simulation speed value(m/s)	Measured speed value(m/s)	Error
1800	160×50	24.29	22.15	8.8%
	160×80	20.77	18.01	13.3%
	160×160	16.49	15.8	4.2%
2000	160×50	25.92	23.3	10.1%
	160×80	21.91	19.98	8.8%
	160×160	17.5	16.6	5.1%

Table 2

Comparison of simulation and measured velocity at different speeds and outlets

2200	160×50	27.53	25.5	7.4%
	160×80	23.31	21.14	9.3%
	160×160	18.81	17.49	7%

Analysis of the improvement of the crushing chamber

- **Improvement to the structure of the cylinder**

It can also be seen from Fig. 4 above that there is a gradient change in pressure at the inlet, when the wind comes in from the inlet, it moves from the inlet to the outlet, and a small part of the wind is discharged from the upper and lower gap between the first row of blades and the wall of the cylinder to continue forward conveying, most of the wind is hindered by the barrier formed by the high speed rotating blades and forms a vortex at the inlet, so that the lentinus edodes stipe cannot continue to be conveyed to the left end with the airflow, making it strike repeatedly at the inlet and concentrate on the right end of the cylinder. To break this phenomenon, an 80mm air inlet is specially opened on the lower cover cylinder at the right end of the lentinus edodes stipe, causing the negative pressure value at the left end to be larger than that at the right end, thus breaking the wind balance at the inlet, so that the lentinus edodes stipe can be transported from the lower right end to the left end due to the pressure gradient, and the lentinus edodes stipe is processed into stipe floss by repeated action with the striking device during the transport process, and finally enters the fan from the outlet under the action of negative pressure.

Fig.13 is the pressure cloud diagram without the lower end air inlet section, from the diagram it can be seen that because the lower end of the cylinder did not open the air inlet, resulting in the lower end does not have pressure gradient distribution, lentinus edodes stipe when being fed from the inlet, due to the existence of no pressure difference, and cannot be discharged from the upper and lower gap of the first row of blades, but has been circling at the entrance, still forming a vortex, unable to discharge, so the machine, in addition to the inlet, also needs to open an air inlet in the lower cover cylinder auxiliary, to break the wind balance and fast discharge.

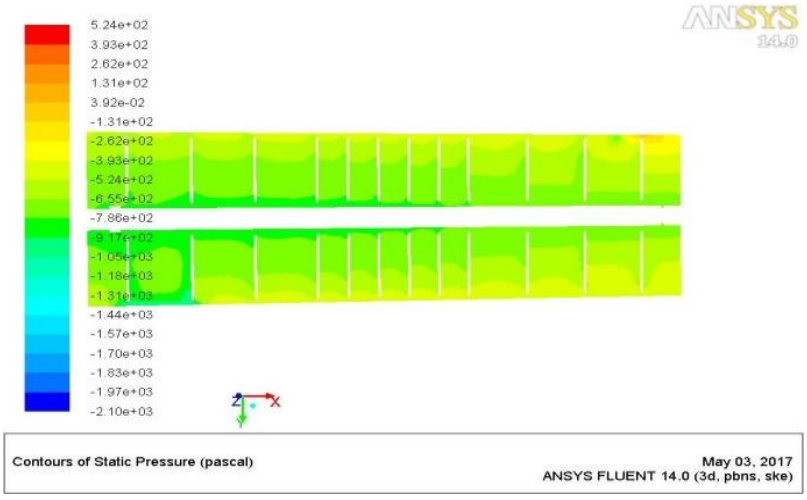

Fig. 13 - Pressure contour plot at plane position Z=-0.03m for no air inlet

- **Improvement of blade structure**

From Fig. 5 and Fig. 6, we can conclude that the airflow speed at the center of the rotor is very small, and the airflow speed in the area swept by the blade is larger. Only one-third of the blades play the role of real striking, and the rest of the blades only play the role of increasing the line speed of the blade tip to improve the quality of the stipe floss, so the structure of the blades can be improved, especially the position of the blades from the tip of one-third. Given the above analysis of the internal flow field of the lentinus edodes stipe into the crushing chamber, the blade structure is now improved by thickening the part of the original straight blade one-third from the tip, increasing 5mm to 8mm, and the improved blade structure is shown in Fig.14.

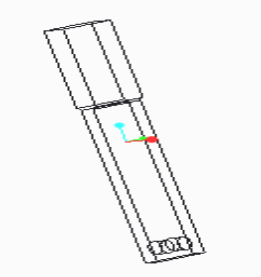

Fig. 14 - Schematic diagram of the improved blade

The turbulent kinetic energy and the transverse velocity gradient and longitudinal velocity gradient were obtained by numerical simulation of the flow fields of these two blades separately without changing other parameters. From Table 3, it can be seen that after the improvement, the turbulent kinetic energy is not only significantly increased, but also the speed gradient is significantly increased, which is more conducive to material conveying and preventing excessive crushing. In addition, the service life of the blades has become longer.

Table 3

Volume average values of turbulent energy for the different blade structure

Blade Structure	Turbulent kinetic energy(m^2/s^2)	Lateral speed gradient(s^{-1})	Longitudinal speed gradient(s^{-1})
Straight Blade	1.665	-90.53	3.2
New blades	2.191	-119.34	2.98

- **Simulation analysis and comparison of flow field for different speed**

Rotational speed is one of the important parameters of machine for lentinus edodes stipe crushing. The higher the speed, the stronger the collision and rubbing between the material and the material, and the greater the centrifugal force on the material, the higher the efficiency, but the higher the energy consumption and the greater the vibration of the machine. Therefore, the smoothness of the discharge as well as the quality of stipe floss formation should be used as a measure to select the appropriate speed under different process conditions.

Keeping the other structural parameters of the model unchanged, the rotational speed of the flow field simulation was changed, and the numerical simulations were performed for the flow fields at 1800 r/min, 2000 r/min, and 2200 r/min, and the volume weighted average value of each energy consumption at different rotational speeds, the velocity gradient values and the maximum negative pressure and maximum velocity values were obtained, as shown in Table 4 and Table 5. Kolmogorov argued that in turbulent flows with large Reynolds number, the energy spectrum of locally isotropic turbulence can be derived by the method of gauge analysis (*Kolmogorovan,1962*).

The only possible form of the dimensionless energy spectrum is Kolmogorov's -5/3 power law (referred to as the -5/3 energy spectrum):

$$E(k) = \alpha \varepsilon^{2/3} k^{-5/3} \tag{4}$$

where:

$E(k)$ is the turbulent energy spectrum, dimensionless; α (also written as Ck) is the Kolmogorov constant; k is the turbulent kinetic energy, m^2/s^2; ε is the turbulent dissipation rate, m^2/s^3.

In terms of velocity gradient, as the speed increases, the value of velocity gradient increases and the shear force between fluids increases. Therefore, based on the energy spectrum and velocity gradient data, the speed of 2000 r/min is selected as a suitable speed value.

Table 4

Volume average values of turbulent energy at different shaft speeds

Rotational Speed (rpm)	V_{max} (m/s)	$-P_{max}$ (Pa)	Turbulent kinetic energy (m^2/s^2)	Turbulent dissipation rate (m^2/s^3)	-5/3 Energy spectrum
1800	42.6	-1329	1.066	343.57	44.10
2000	46	-1506	1.159	415.18	43.52
2200	49.5	-1699	1.274	498.15	41.97

Table 5

Volume average values of velocity gradient at different shaft speeds

Rotational Speed (rpm)	Transverse fluid velocity gradient (s^{-1})	Longitudinal fluid velocity gradient (s^{-1})
1800	-69.63	2.66
2000	-81.34	2.75
2200	-95.4	2.88

- **Simulation analysis and comparison of flow field for different outlet areas**

The size of the outlet area mainly affects the air volume of the suction fan, and the size of this air volume has a great influence on the discharge of lentinus edodes stipe floss and the quality of the stipe floss. If the outlet area is too large, the air volume becomes large, and the material stays in the crushing chamber for a smaller time, which affects the quality of the stipe floss; if the outlet area is too small, the air volume is not enough, which affects the discharge of the material, so that the material that reaches the quality requirement cannot be discharged in time. So, the area of the outlet should have a suitable value.

The simulation model is changed, the outlet area is changed, and the simulation analysis and comparison are carried out for different outlet areas respectively, and the volume-weighted average value of energy consumption parameters and velocity gradient distribution of the three outlet areas are obtained, as shown in Table 6. As shown in Table 6, with the increase of the outlet area, the turbulent kinetic energy of the flow field inside the crushing chamber increases, and the turbulent energy spectrum decreases, i.e., the effective energy utilization decreases, the turbulent dissipation rate increases, the maximum negative pressure increases, and the maximum linear velocity decreases.

However, as far as the outlet flow rate is concerned, the outlet flow rate was 0.191 kg/s, 0.245 kg/s, and 0.31 kg/s with the increase of the outlet area, respectively, in increasing. And in terms of Table 7 velocity gradient, the transverse velocity gradient decreases as the outlet port area increases, which is not conducive to the transport of lentinus edodes stipe floss, so on comprehensive consideration, the outlet port area of 160×80 mm^2 is selected as a suitable outlet port area parameter.

Table 6

Volume average values of turbulent energy for the different discharge area

Area (mm^2)	V_{max} (m/s)	$-P_{max}$ (Pa)	Turbulent kinetic energy (m^2/s^2)	Turbulent dissipation rate (m^2/s^3)	-5/3 Energy spectrum
160×50	52.4	-1414	1.018	395.02	52.26
160×80	49.5	-1699	1.274	498.15	41.97
160×160	47	-2296	1.665	663.52	32.52

Table 7

Volume average values of velocity gradient for the different discharge area

Area (mm^2)	Transverse fluid velocity gradient (s^{-1})	Longitudinal fluid velocity gradient (s^{-1})
160×50	-99.98	2.78
160×80	-95.4	2.88
160×160	-90.53	3.2

CONCLUSIONS

(1) Using FLUENT14.0 software to simulate and analyze the flow field inside the crushing chamber of machine for lentinus edodes stipe crushing, the flow field distribution state and basic characteristics of the internal flow field of the crushing chamber, the main working part of the machine for lentinus edodes stipe crushing, were obtained through the simulation analysis of the flow field inside the crushing chamber, and the visualization of the flow field of the complex crushing chamber was realized.

From various cloud diagrams, it can be seen that the flow field velocity increases with the increase of radius until it reaches the cylinder wall velocity quickly will be 0, and the pressure on the backwind side of the blade is greater than that on the windward side. And a detailed theoretical analysis of the opening of the air inlet at the lower end of the cylinder was carried out, and it was concluded that the opening of the air inlet at the lower end could effectively improve the pressure state inside the crushing chamber, break the wind balance at the inlet, and promote the conveying of materials.

(2) By comparing the experimental values obtained from the actual measurement of the velocity at the discharge port and the velocity between the blades at different rotational speeds and different discharge port areas with the simulated values obtained from the simulation of the flow field in the crushing chamber using FLUENT software, it is concluded that the error between the simulated data values and the actual measured values is within 10%, which indicates that the simulation analysis is feasible.

(3) By analyzing the flow field, the problems of the flow field are derived, and then the pelletizing cylinder is improved. In other words, according to the simulation results obtained from the simulation of the crushing chamber with different speed, blade structure, outlet area and structure, and combined with the evaluation indexes such as turbulent kinetic energy, turbulent energy spectrum, velocity gradient, outlet flow rate and maximum velocity and maximum negative pressure, it is concluded that under the conditions of 2000r/min speed, 160×80 mm^2 outlet area and new blade, the flow field in the crushing chamber The turbulence energy of the new blade is greater and the velocity gradient is higher, which is more conducive to the conveying of materials, and provides a theoretical basis for further optimization of the crushing machine.

ACKNOWLEDGEMENT

This research was developed within the framework of the project “China Machinery Industry Group Co., Ltd. Major science and technology”.

REFERENCES

[1] Aghaei Tog R., Tousi A.M., Tourani A., (2008), Comparison of turbulence methods in CFD analysis of compressible flows in radial turbomachines, *Aircraft Engineering and Aerospace Technology*, *80*(6), 657-665.

[2] Bo Yuan Lim, Rosnah Shamsudin, B.T. Hang Tuah Baharudin, (2016), Performance evaluation and CFD multiphase modeling for Multistage Jatropha Fruit Shelling Machine, I*ndustrial Crops and Products, 85,* 125-138.

[3] Cao Liying, Wu Pei, Ma Yanhua, (2010), Analysis on single-phase flow field of hammer mill based on FLUENT, *Cereal & Feed Industry*, (12), 45-47.

[4] Cao Yuan, Wang Jianxin, Cao Liying, (2015), Optimization anysis of a new feed mill structure based on fluent, *Feed Industry*, *36*(3), 5-8.

[5] Darelius Anders, Rasmuson Anders, Van Wachem Berent, (2008), CFD simulation of the high shear mixing process using kinetic theory of granular flow and frictional stress models, *Chemical Engineering Science*,*63*(8):2188-2197.

[6] Dennis Lammers, (2005). *Determination of the air and crop flow behavior in the blowing unit and spout of a pull -type forage harvester*, Saskatchewan: University of Saskatchewan.

[7] Fabien Barailler, Mourad Heniche, Philippe A, (2006), CFD analysis of a rotor-stator mixer with viscous fluids, *Chemical Engineering Science*, *61*(9):2888-2894.

[8] Gong Jun, Song Yongqi, Guo Runlan, (2006), Numerical simulation of flow on a new model of comminuting mill, *Modern Manufacturing Engineering*, (11), 97-99.

[9] Guo Yuhang, (2015), *Numerical Simulation of Gas Solid Two Phase Flow Vertical Screw Conveyor*, Taiyuan: Taiyuan University of Science & Technology.

[10] Huang Yihui, (2011), *Study on O-SEPA Classifier’s Structure and Its Fluid Field Characteristics*, Wuxi: Jiangnan University.

[11] Kolmogorovan, (1962), A refinement of previous hypotheses concerning the local structure of turbulence in incompressible viscous fluid for very large Reynolds number, *Journal of fluid mechanics*, *13*(1), 82-85.

[12] Li Weidong, Yao Qi, (2017), Optimization analysis for impeller inlet of artificial heart pump with hydraulic suspension based on CFD, *Beijing Biomedical Engineering*,*36*(1):21-28.

[13] Liu Liangdong, (2016), *Design and Experimental Test of a Machine for Processing lentinus edodes stipe into floss*, Wuhan: Hua Zhong Agricultural University.
[14] Min Jin, Chunguang Wang, Pengpeng Wang, (2020), CFD Numerical simulation of temperature and airflow distribution in pigsty based on grid independence verification, *INMATEH Agricultural Engineering, 61*(2), 241-250.
[15] Qianpu Wang, Morten Chr., Melaaen, Sunil R., De Silva, (2001), Investigation and simulation of a cross-flow air classifier, *Powder technology*, *120*(3), 273-280.
[16] Pei Yaowu, (2014), *Simulation and Analyzation on Flow Field in Crashing Cavity of New-type Feed Hammer Mill*, Baotou:Inner Mongolia University of Science&Technology.
[17] Robert Johansson, Magnus Evertsson, (2014), CFD simulation of a centrifugal air classifier used in the aggregate industry, *Minerals Engineering*, *63*, 149-156.
[18] Shang Tan, Guo Guisheng, (2014), *Analysis of Fluid-structure Interaction and Simulation of Internal Flow Field for Cornstalk Rubbing Silk Machine,* Yangling: Northwest A&F University.
[19] Shen Peiyu, Zhao Hao, Zhang Yuzhong, (2010), Numerical simulation of fluid field for high-speed cutting grinding, *Transactions of the Chinese Society for Agricultural Machinery*,*41*(09):60-65.
[20] Song Yongqi, (2007), *Numerical Simulation on Superfine Comminuting Mill with Turbulence*, Lanzhou: Lanzhou University of Technology.
[21] Wang Xiaofeng, (2008), *Study on the Flow Patterns of Comminuting Process in a Superfin*, Wuxi: Jiangnan University.
[22] Wang Juan, Wang Chunguang, Wang Fang, (2010), Numerical simulation on three-dimensional turbulence air flow of 9R-40 rubbing and breaking machine based on Fluent software, *Transactions of the CSAE*, *26*(2), 165-169.
[23] Zhai Zhiping, Wang Chunguang, (2008), Numerical simulation and optimization for air flow in an impeller blower, *Transactions of the Chinese Society for Agricultural Machinery*, (06),84-87.
[24] Zhang Hongwei, (2013), *Numerical Simulation and Experimental Measurement of Single-phase Turbulent Flow in Stirred Media Mill*, Guangzhou: South China University of Technology.
[25] Zhu Lianhua, Song Qiang, Ze Xiangbo, (2013), Numerical simulation of the flow field of household soybean milk machine with the S shape blade, *Special Topics on Structure and Design Appliances,* (9), 60-62.
[26] Zong Quanli, Zheng Tiegang, Liu Huanfang, (2013), Numerical simulation and analysis on whole flow field for drip self-cleaning screen filter, *Transactions of the Chinese Society of Agricultural Engineering, 29*(16), 57-65.